Anal. Chem. **2007,** *79,* 7845−7852

Ion Funnel Trap Interface for Orthogonal Time-of-Flight Mass Spectrometry

Yehia Ibrahim, Mikhail E. Belov,* Aleksey V. Tolmachev, David C. Prior, and Richard D. Smith

Biological Sciences Division, Pacific Northwest National Laboratory, P.O. Box 999, Richland, Washington 99352

A combined electrodynamic ion funnel and ion trap coupled to an orthogonal acceleration (oa)-time-of-flight mass spectrometer was developed and characterized. The ion trap was incorporated through the use of added terminal electrodynamic ion funnel electrodes enabling control over the axial dc gradient in the trap section. The ion trap operates efficiently at a pressure of ~1 Torr, and measurements indicate a maximum charge capacity of ~3 × 10^7 charges. An order of magnitude increase in sensitivity was observed in the analysis of low concentration peptides mixtures with orthogonal acceleration (oa)-time-of-flight mass spectrometry (oa-TOF MS) in the trapping mode as compared to the continuous regime. A signal increase in the trapping mode was accompanied by reduction in the chemical background, due to more efficient desolvation of, for example, solvent related clusters. Controlling the ion trap ejection time was found to result in efficient removal of singly charged species and improving signal-to-noise ratio (S/N) for the multiply charged analytes.

The orthogonal acceleration time-of-flight mass spectrometer is a powerful platform for fast on-line detection of biopolymers. Orthogonal acceleration (oa)-time-of-flight mass spectrometry (oa-TOF MS) is characterized by unsurpassed speed of analysis, high sensitivity, high mass measurement accuracy, and high mass resolving power,[1−5] and thus, representing an attractive platform for high throughput analyses. Because of the inherently pulsed separation of ions in a TOF flight tube, the efficient coupling of a continuous ion source, such as electrospray ionization (ESI), to TOF MS is challenging. Considering the pioneering work by Dodonov et al.,[5,6] ESI-oa-TOF MS has been widely applied[7,8] and successfully commercialized. However, the sensitivity of ESI-oa-TOF MS is limited by the instrument duty cycle, which depends on the mass-to-charge ratio (m/z) of the detected analytes and typically remains within 5−20%. Increasing the instrument duty cycle, e.g., by using higher pulsing frequency, reduces the detectable m/z range.

Various ion traps, such as 3D, linear quadrupole, and ring electrode traps,[9−14] have been introduced between the ESI source and a TOF MS to effectively accumulate ions prior to analysis.[15] When coupling an ion trap to a TOF instrument, three key characteristics should be considered: trapping efficiency, charge capacity of the trap, and the speed of ion ejection from the trap. Increasingly being used are the linear ion traps for their capabilities that are similar to those of 3D traps but with higher charge capacity.[16] However, these traps are limited by lower operating pressures (usually within 10^{-5}−10^{-3} Torr). Since both trapping efficiency and collisional relaxation (i.e., ion cooling) are directly proportional to the number density of the collision gas, accumulation of ions at higher pressures potentially offers higher sensitivity. An ion trap that works at a pressure of several Torr is also particularly beneficial for use with gas-phase ion separations, such as ion mobility spectrometry (IMS), coupled to TOF MS. Efficient implementation of a higher charge capacity ion trap prior to IMS would increase overall sensitivity, otherwise constrained by the low IMS duty cycle associated with pulsed ion introduction. Though segmented quadrupoles were shown to operate at pressures of 0.1−3.0 Torr,[17] higher order multipoles provide greater radial confinement[18] and, given the dependence of the effective potential on pressure,[19] are better suited for trapping

* Corresponding author. Dr. Mikhail Belov, Pacific Northwest National Laboratory, P.O. Box 999/MS K8-98, Richland, WA 99352; e-mail: mikhail.belov@pnl.gov.

(1) Verentchikov, A. N.; Ens, W.; Standing, K. G. *Anal. Chem.* **1994**, *66*, 126−133.
(2) Morris, H. R.; Paxton, T.; Dell, A.; Langhorne, J.; Berg, M.; Bordoli, R. S.; Hoyes, J.; Bateman, R. H. *Rapid Commun. Mass Spectrom.* **1996**, *10*, 889−896.
(3) Guilhaus, M.; Selby, D.; Mlynski, V. *Mass Spectrom. Rev.* **2000**, *19*, 65−107.
(4) Wolff, J. C.; Eckers, C.; Sage, A. B.; Giles, K.; Bateman, R. *Anal. Chem.* **2001**, *73*, 2605−2612.
(5) Dodonov, A. F.; Kozlovski, V. I.; Soulimenkov, I. V.; Raznikov, V. V. *Eur. J. Mass Spectrom.* **2000**, *6*, 481−490.
(6) Mirgorodskaya, O. A.; Shevchenko, A. A.; Chernushevich, I. V.; Dodonov, A. F.; Miroshnikov, A. I. *Anal. Chem.* **1994**, *66*, 99−107.
(7) Chernushevich, I. V.; Ens, W.; Standing, K. G. *Anal. Chem.* **1999**, 452A−461A.
(8) Chernushevich, I. V.; Thomson, B., MDS Inc. MS/MS Scan Methods for a Quadrupole/Time of Flight Tandem Mass Spectrometer. U.S. Patent 6,-507,019, January, 14, 2003.
(9) Michael, S. M.; Chien, B. M.; Lubman, D. M. *Anal. Chem.* **1993**, *65*, 2614−2620.
(10) Purves, R. W.; Li, L. *J. Am. Soc. Mass Spectrom.* **1997**, *8*, 1085−1093.
(11) Doroshenko, V. M.; Cotter, R. J. *J. Mass Spectrom.* **1998**, *33*, 305−318.
(12) Campbell, J. M.; Collings, B. A.; Douglas, D. J. *Rapid Commun. Mass Spectrom.* **1998**, *12*, 1463−1474.
(13) Luca, A.; Schlemmer, S.; Čermák, I.; Gerlich, D. *Rev. Sci. Instrum.* **2001**, *72*, 2900−2908.
(14) Collings, B. A.; Campbell, J. M.; Mao, D.; Douglas, D. J. *Rapid Commun. Mass Spectrom.* **2001**, *15*, 1777−1795.
(15) Dresch, T.; Gulcicek, E. E.; Whitehouse, C., Analytica of Branford, Inc. Ion Storage Time-of-Flight Mass Spectrometer. U.S. Patent 6,020,586, February 1, 2000.
(16) Loboda, A.; Krutchinsky, A.; Loboda, O.; McNabb, J.; Spicer, V.; Ens, W.; Standing, K. *Eur. J. Mass Spectrom.* **2000**, *6*, 531−536
(17) Dodonov, A.; Kozlovsky, V.; Loboda, A.; Raznikov, V.; Sulimenkov, I.; Tolmachev, A.; Wollnik, A. K. H. *Rapid Commun. Mass Spectrom.* **1997**, *11*, 1649−1656.

10.1021/ac071091m CCC: $37.00
Published on Web 09/13/2007

larger ion populations at higher pressures. Several groups have reported on efforts to improve the efficiency of ion ejection from traps, which operate at intermediate pressures of $10^{-5}-10^{-3}$ Torr, by segmenting the quadrupole rods,[17,20] adding resistively coated electrodes around the trap,[13] using conical rods,[21] or inserting sloped T-shaped rods between multipole rods.[22]

Particularly attractive for fast ion ejection is a "stacked-ring" assembly, which is similar to the high-order multipole and has been thoroughly characterized both analytically and experimentally.[13,18] The "stacked-ring" ion trap is comprised of ring-shaped electrodes where 180° phase-shifted rf fields are applied to adjacent electrodes to create a radial confining field. Axial confinement is achieved by applying dc potentials to the trap terminus. To improve ion ejection, an axial dc field is generated by superimposing a pulsed gradient onto the rf field. The effective potential force in the "stacked-ring" assembly depends on the distance between adjacent electrodes and increases exponentially on approaching the electrode edges.[18] At a sufficiently small gap between the electrodes, such a device can provide highly efficient rf-confinement. Another advantage is that generation of a pulsed gradient in an assembly of ring electrodes for fast ion ejection is also highly effective.

A modification of the "stacked-ring" assembly is the electrodynamic ion funnel,[23] which is characterized by ring electrodes of progressively reduced inner diameters that serve to collimate a diffuse ion beam. Introduced and significantly enhanced by our laboratory for ion sampling from ESI sources,[23−26] the electrodynamic ion funnel improves ion utilization compared to standard skimmer-based MS interfaces. Since it can efficiently operate at pressures of ∼1−30 Torr,[27] the ion funnel represents an attractive interface with higher pressure ionization sources.

An important aspect of ion trap operation relates to its ability to reduce "chemical background" while enhancing the analyte signal, which leads to an increase in signal-to-noise ratios. Improving the signal-to-noise ratio (S/N) is critical for biological experiments with, for example, human blood plasma in which biological applications (e.g., disease biomarkers) are often present at very low concentrations among higher abundance analytes and chemical background. Chemical background can arise due to many factors, and in some cases it can be due to singly charged partially solvated ions that typically generate abundant signals at the low m/z range of a mass spectrum.[28] The presence of such species is a result of a compromise typically made in the ESI interface between conditions that provide good desolvation but that also avoid analyte activation/dissociation. Although MS-based methods for separating multiply charged analytes from singly charged species have been developed to reduce chemical background, these approaches are limited by either low duty cycle or pronounced losses of doubly charged species under the conditions used to suppress singly charged ions.[29,30]

In the present work, we have characterized an electrodynamic ion funnel trap at a pressure of ∼1 Torr. The electrodynamic ion funnel was coupled to a high-performance oa-TOF mass spectrometer, which was operated in both trapping and continuous modes for comparison. Analysis of peptide mixtures with oa-TOF MS in the trapping mode revealed reduction in the chemical background as well as significant improvements in the S/N of the analyte species.

EXPERIMENTAL SETUP

The experiments were performed using a prototype dual-stage reflectron oa-TOF mass spectrometer as shown schematically in Figure 1a. Ions from the electrospray source were transmitted through a 508 μm i.d., 10 cm long stainless steel capillary interface, resistively heated to 165 °C, and into an electrodynamic ion funnel that worked at pressure of ∼1 Torr. A schematic diagram of the ion funnel is depicted in Figure 1b. The 180° phase-shifted rf fields were applied to adjacent ring-electrodes at a peak-to-peak amplitude of 70 V_{p-p} and a frequency of 600 kHz. Ion transmission through the funnel was improved by superimposing a dc field onto the rf field applied to each electrode. In the continuous mode, the dc gradient applied to the funnel was 20 V/cm.

The funnel consists of 98 brass ring electrodes, each electrode 0.5 mm thick and separated 0.5 mm apart with Teflon spacers. The ring electrodes are assembled onto four ceramic rods that ensure proper alignment. The inner diameters of the ring electrodes vary from 25.4 mm at the funnel entrance, 19.1 mm at the trap section (between grids G1 and G2 in Figure 1b), and 2.4 mm at the funnel exit plate. Section 1 of the ion funnel in Figure 1b, which accepts ions exiting the heated capillary, is composed of 24 ring electrodes, each having a 25.4 mm i.d. A jet disrupter made of a 6.5 mm brass disk is located ∼20 mm downstream of the funnel entrance to reduce the gas load to the subsequent stages of differential pumping while maintaining high ion transmission.[31] An independent dc voltage was applied to the jet disrupter. The pressure in the ion funnel trap was measured using a convectron gauge (Granville-Phillips, Boulder, CO) directly mounted on the ion funnel chamber. The Teflon spacers between the funnel ring electrodes ensured that the ion funnel pressure matched that of the ambient gas in the ion funnel chamber.

The ions exiting section 1 were collimated into section 2, which is characterized by a converging geometry (Figure 1b). Section 3, which is characterized by diverging geometry, couples section 2 to the ion trap and is separated from section 2 by a 3 mm orifice.

(18) Gerlich, D. In *State-Selected and State-to-State Ion-Molecule Reaction Dynamics. Part 1. Experiment*; Ng, C.-Y., Baer, M., Eds.; Wiley: New York, 1992; Vol. 82, pp 1−176.
(19) Tolmachev, A. V.; Chernushevich, I. V.; Dodonov, A. F.; Standing, K. G. *Nucl. Instrum. Methods Phys. Res., Sect. B* **1997**, *124*, 112−119.
(20) Belov, M. E.; Nikolaev, E. N.; Harkewicz, R.; Masselon, C. D.; Alving, K.; Smith, R. D. *Int. J. Mass Spectrom.* **2001**, *208*, 205−225.
(21) Mansoori, B. A.; Dyer, E. W.; Lock, C. M.; Bateman, K.; Boyd, R. K.; Thomson, B. A. *J. Am. Soc. Mass Spectrom.* **1998**, *9*, 775−788.
(22) Taban, I. M.; McDonnell, L. A.; Rompp, A.; Cerjak, I.; Heeren, R. M. A. *Int. J. Mass Spectrom.* **2005**, *244*, 135−143.
(23) Shaffer, S. A.; Tang, K.; Anderson, G. A.; Prior, D. C.; Udseth, H. R.; Smith, R. D. *Rapid Commun. Mass Spectrom.* **1997**, *11*, 1813−1817.
(24) Kim, T.; Tolmachev, A. V.; Harkewicz, R.; Prior, D. C.; Anderson, G. A.; Udseth, H. R.; Smith, R. D.; Bailey, T. H.; Rakov, S.; Futrell, J. H. *Anal. Chem.* **2000**, *72*, 2247−2255.
(25) Belov, M. E.; Gorshkov, M. V.; Udseth, H. R.; Anderson, G. A.; Smith, R. D. *Anal. Chem.* **2000**, *72*, 2271−2279.
(26) Tolmachev, A. V.; Kim, T.; Udseth, H. R.; Smith, R. D.; Bailey, T. H.; Futrell, J. H. *Int. J. Mass Spectrom. Ion Processes* **2001**, *203*, 31−47.
(27) Ibrahim, Y.; Tang, K.; Tolmachev, A. V.; Shvartsburg, A. A.; Smith, R. D. *J. Am. Soc. Mass Spectrom.* **2006**, *17*, 1299−1305.
(28) Cech, N. B.; Enke, C. G. *Mass Spectrom. Rev.* **2001**, *20*, 362−387.
(29) Thomson, B. A.; Chernushevich, I. V. *Rapid Commun. Mass Spectrom.* **1998**, *12*, 1323−1329.
(30) Chernushevich, I. V.; Fell, L. M.; Bloomfield, N.; Metalnikov, P. S.; Loboda, A. V. *Rapid Commun. Mass Spectrom.* **2003**, *17*, 1416−1424.
(31) Kim, T.; Tang, K.; Udseth, H. R.; Smith, R. D. *Anal. Chem.* **2001**, *73*, 4162−4170.

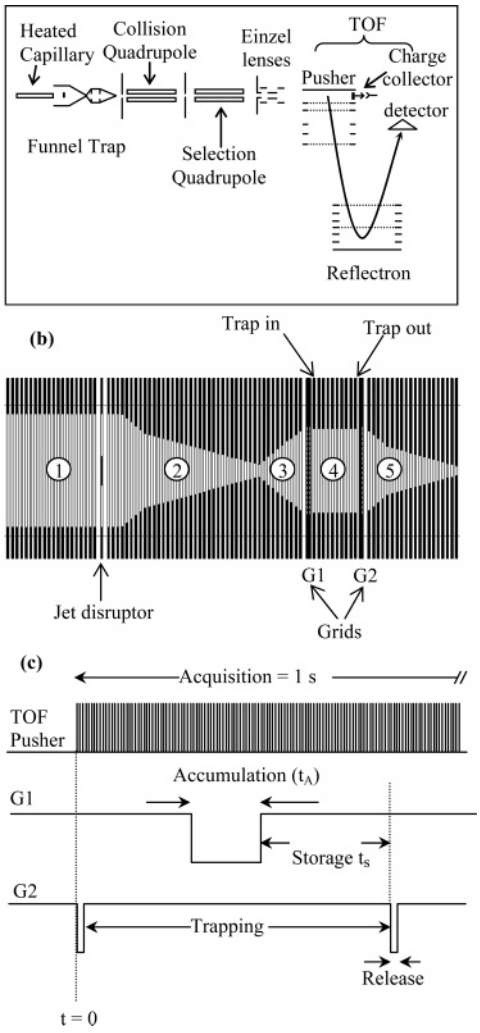

Figure 1. (a) Outline of experiment setup. (b) Schematic diagram of the ion funnel trap. The numbers refer to the different sections of the funnel (see text). (c) The pulse sequence for ion accumulation, storage, and ejection from the trap.

In the trapping mode, ions are accumulated in section 4, which is comprised of 10 ring electrodes, each having a 19.1 mm i.d. The trapping region (section 4) is separated from sections 3 and 5 by two grids fabricated from 95%-transmission nickel mesh (InterNet Inc., Minneapolis, MN).

Pulsing voltages applied to the grids G1 and G2 were used to control ion populations that could be introduced into the trap, as well as to control the ion storage and extraction times, respectively. The dc gradient in the trapping region was varied independently from the rest of the ion funnel by adjusting potentials at the first ("Trap in") and last electrodes ("Trap out") in section 4. In the continuous mode, the potentials on grids G1 and G2 were optimized to ensure efficient ion transmission through the trapping region. The ions passing section 4 were recollimated in the tapered portion of section 5 and then focused into a 15 cm long collisional quadrupole, operating at a pressure of $\sim 6 \times 10^{-3}$ Torr.

After collisional relaxation and focusing, ions were transmitted through a 20 cm long selection quadrupole at a pressure of 1.5×10^{-5} Torr and focused by an Einzel lens assembly into a TOF extraction region. Both the collisional and selection quadrupoles were operated at an rf amplitude of 2500 V_{p-p} and an rf frequency of 2 MHz. The TOF chamber encompasses a stack of acceleration electrodes, a dual-stage ion mirror, and a 40 mm diameter extended dynamic range bipolar detector, having a 10 μm pore size and 12° ± 1 bias angle (Burle ElectroOptics, Sturbridge, MA). The length of the TOF flight tube is 100 cm, and the distance between the center of the 40 mm long TOF extraction region and the detector axis is 75 mm. A typical full width at half-maximum (fwhm) of signal peaks was 3.0−3.5 ns, yielding an optimum resolving power of 10 000 and a routine resolving power of 7000−8000. The TOF detector was impedance matched to a 2 GS/s 8-bit analog-to-digital converter AP200 (Acqiris, Geneva, Switzerland) that enabled routine mass measurement accuracy of ~5 ppm. Prior to ion introduction into the TOF acceleration stack, both continuous and pulsed ion currents were measured with a Faraday cup charge collector positioned on the interface axis immediately downstream of the TOF extraction region (Figure 1a). Ion current pulses were acquired using a fast current inverting amplifier (Keithley model 428, Cleveland, OH) coupled to a digital oscilloscope (Tektronix, Richardson, TX).

The pulsing sequence for ion trapping is schematically depicted in Figure 1c. With one of the TOF MS control bits (Run/Stop) toggled high at the beginning of each spectrum acquisition, a waveform generator (Hewlett-Packard, Palo Alto, CA) was triggered to release a burst of trigger pulses. The repetition rate and the number of burst pulses determined the trapping and acquisition times, respectively. Each trigger pulse activated a delay generator (Stanford Research Systems, San Jose, CA), which in turn determined the pulse widths and time delay in pulsing grids G1 and G2. The output TTL signals from the delay generator were then fed into two independent high-voltage switches (Behlke, Kronberg, Germany) that provided pulsed voltages for the two pulsing grids. For the experiments reported herein, grid G1 was not pulsed and ESI-generated ions entered the trap continuously.

Peptide samples were purchased from Sigma-Aldrich (Sigma-Aldrich, St. Louis, MO), prepared in 50% aqueous methanol acidified with 1% acetic acid and used without further purification. Polyethylene glycol/ultramark mixture was obtained from Thermo (Thermo Scientific, San Jose, CA) and prepared in a water/acetonitrile solution (20:80 v:v). The samples were infused into the mass spectrometer at a flow rate of 0.4 μL/min.

RESULTS AND DISCUSSION

The ion funnel was initially optimized by adjusting the rf and dc fields in the trap region for higher sensitivity. Figure 2 shows the average monoisotopic intensity of triply charged neurotensin as a function of the rf amplitude at a constant rf frequency of 600 kHz. Although an optimum was found for the rf amplitude in the trapping mode, no significant signal variation was observed over a wide range of rf amplitudes in the continuous mode. Therefore, 55 V_{p-p} was used as the optimal rf amplitude for the results reported here. The optimum rf amplitude was also found to be consistent with relationships reported recently.[32] The relationship for high m/z limit $(m/z)_{high}$ as a function of the rf frequency f and the radial dc electric field component E_n can be estimated as follows:

$$(m/z)_{high} = eV_{RF}^{2} \exp(-2h_0/\delta)/2m_u\omega^2\delta^3E_n \qquad (1)$$

Here, e is the elementary charge, $m_u = 1.6605 \times 10^{-27}$ kg is the atomic mass unit, $\omega = 2\pi f$ is the angular frequency, $h_0 \approx 0.5$ mm

(32) Page, J. S.; Tolmachev, A. V.; Tang, K.; Smith, R. D. *J. Am. Soc. Mass Spectrom.* **2006**, *17*, 586−592.

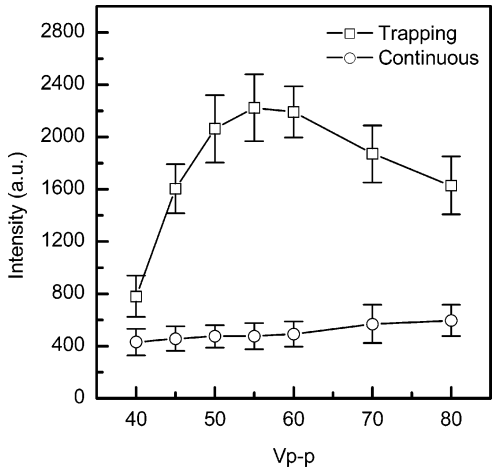

Figure 2. Comparison of monoisotopic $[M + H_3]^{3+}$ signal intensities from ESI of a 5 nM neurotensin solution in the continuous and trapping modes. Intensity is plotted as a function of the funnel rf amplitude at constant rf frequency of 600 kHz. Similar results were obtained for angiotensin I $[Ang\ I + H_2]^{2+}$ and fibrinopeptide A $[Fib\ A + H_2]^{2+}$ ions. Accumulation time = 100 ms, extraction time = 45 μs.

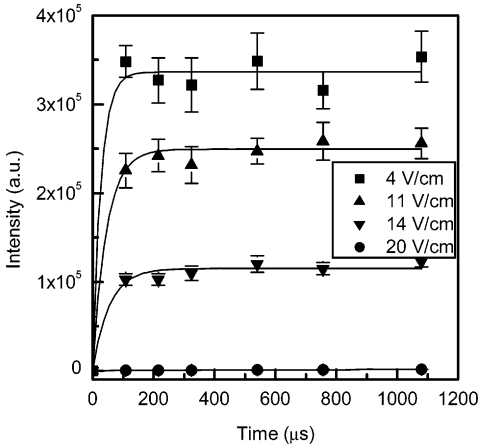

Figure 3. Monoisotopic $[M + H]^+$ peak intensity from ESI of a 1 μM reserpine solution as a function of the extraction time for four dc gradients in the trap region.

is the distance corresponding to the onset of ion losses on the surface of the ion funnel ring electrodes, and δ is related to the distance between the ring electrodes, d = 1 mm, as $\delta = d/\pi$. Assuming that the trapped ion ensemble is limited to $(m/z)_{high} \approx$ 2000 amu, using f = 600 kHz and the electric field characteristic for the dc trapping conditions in our experiments, E_n = 20 V/cm, one can obtain from eq 1 the rf voltage $V_{RF} \approx$ 30V, or 60 V_{p-p}, which is consistent with the experimentally observed rf amplitude (Figure 2). In the continuous mode, both dc trapping and space charge components of E_n are reduced, which explains the different V_{RF} behavior in Figure 2.

We have also found that trapping efficiency strongly depends on the axial dc gradient. Figure 3 shows the dependence of reserpine monoisotopic peak intensity on the extraction time at four different dc gradients in the trap region. Using a dc gradient of 20 V/cm (which is similar to that employed in the rest of the ion funnel) led to poor ion accumulation efficiency. Reduction of the dc gradient from 20 to 4 V/cm resulted in a more than 2 orders of magnitude improvement in sensitivity and an ion extraction time of 100 μs. Fast removal of ions from the trap is important for efficient coupling of the ion trap to the oa-TOF mass spectrometer.

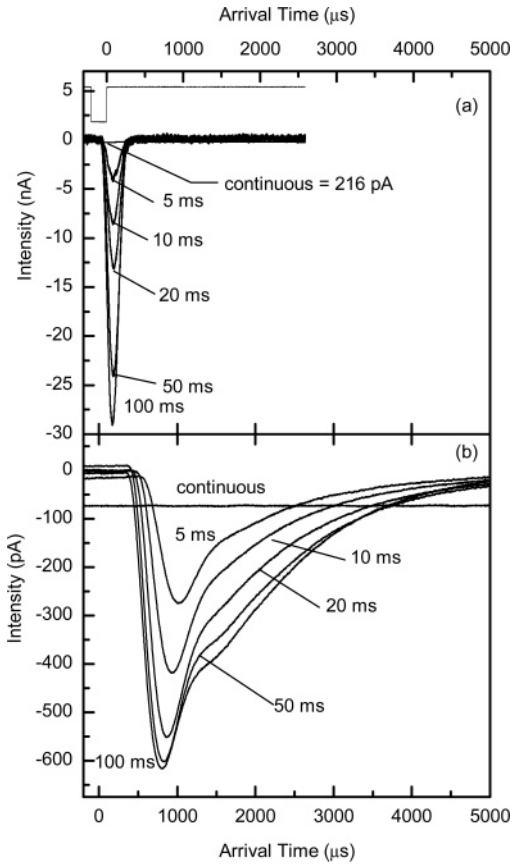

Figure 4. Current pulse measurements for ESI of a 1 μM reserpine solution at various accumulation times. (a) Current at the collisional quadrupole. (b) Current at the charge collector. Extraction time was 200 μs. Note that the intensity unit is nA for panel a and pA for panel b.

Figure 3 indicates that lower dc gradients give rise to more efficient ion accumulation while higher dc gradients resulted in lower trapping efficiency. The drastic decrease in ion accumulation efficiency with an increase in the ion trap dc field is related to axial compression of the ion cloud and associated space charge effects. Because of the cylindrical geometry of the trap, the dc trapping field has a radial component that tends to eject ions in the radial direction where they experience higher rf oscillations and are lost to the electrodes. When the axial electric field is sufficiently low (4 V/cm), the accumulated ion cloud extends axially, thus increasing the trap capacity and its efficiency. Additional evidence from SIMION simulations is provided in the Supporting Information.

The ion current was measured at the collisional quadrupole and the charge collector (Figure 1a) in both the trapping and continuous modes. Comparison of the observed ion current signals on these two elements provides insight into transmission efficiency through the quadrupole interface and electrostatic ion optics. In addition, an estimate of trapping efficiency can be made based on comparison of ion signals at the collisional quadrupole in continuous and trapping modes. Figure 4a shows the ion current measured at the collisional quadrupole rods obtained from ESI of a 1 μM solution of reserpine. Ion current pulses were acquired at different accumulation times in the ion trap. Note the maximum amplitude of the ion current pulse (28 nA at 100 ms accumulation time) exceeded that of the continuous beam (216 pA) by more

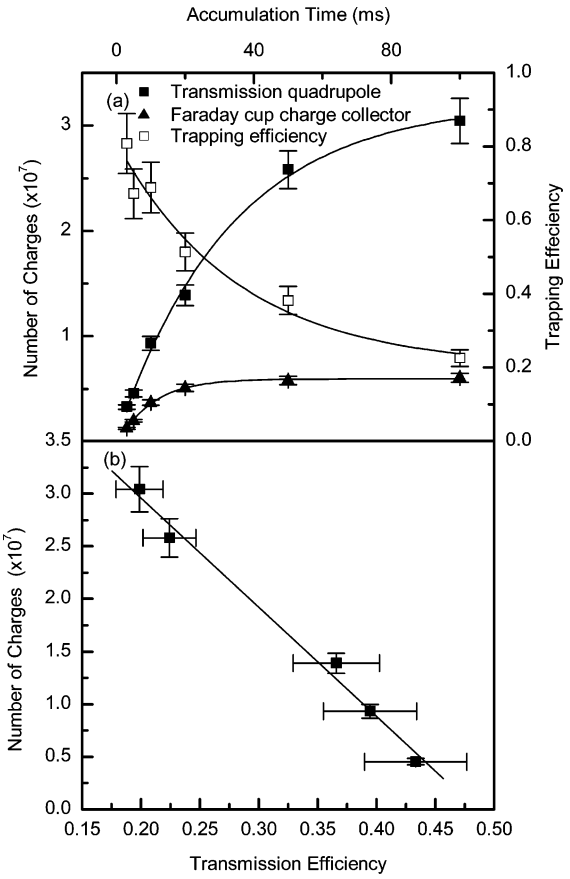

Figure 5. (a) Number of charges detected at the collisional quadrupole (■) and charge collector (▲) as calculated from the areas under the traces shown in Figure 4. (b) Transmission efficiency through the quadrupole interface as calculated from the ratio of the number of charges at the collisional quadrupole and charge collector in Figure 5a.

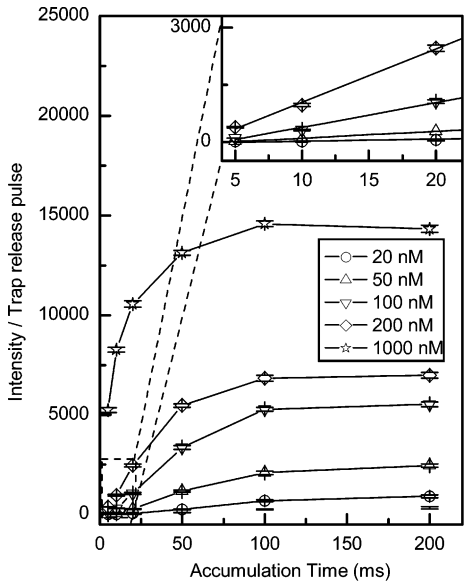

Figure 6. Monoisotopic $[M + H]^+$ peak intensity for ESI of a reserpine solution normalized to the number of trap release pulses per 1 s acquisition time as a function of accumulation time at different concentrations. The inset shows the linear dynamic range of the trap. Note that error bars are too small to be observed.

than 2 orders of magnitude. Figure 4b shows both pulsed and continuous ion currents at the charge collector obtained with the same solution. The traces in Figure 4b have a full width at half-maximum (fwhm) of ~1−2 ms as compared to ~200 μs for the traces shown in Figure 4a, reflecting diffusion broadening of the ion current pulse in the collisional quadrupole. The reason for the lower ion currents at the charge collector is explained below.

The number of charges released from the ion trap was calculated from the areas under the traces in Figure 4a and is plotted as ■ in Figure 5a. The number of charges increases as the accumulation time increases. While the total number of charges reaches ~3×10^7, the linear range for the ion trap extends to only ~1×10^7 charges. The trapping efficiency (depicted in Figure 5a as □) was calculated as the ratio of the charge impinging on the collisional quadrupole rods after a single accumulation event to the charge delivered to the same quadrupole by the continuous beam over the same accumulation period (see Figure 4a). The trapping efficiency reached 70−80% at shorter accumulation times (<10 ms) and then decreased to 20−30% on approaching the charge capacity of the trap (for accumulation time > 50 ms). The ion losses at the charge collector were due to reduction of ion transmission from the collision quadrupole to the charge collector. Figure 5b shows the transmission efficiency of the quadrupole and focusing ion optics interface in detecting pulsed ion currents at the charge collector. Transmission efficiency was determined as the ratio of the pulsed ion current (expressed as number of charges) at the charge collector to the pulsed ion current at the collisional quadrupole rods in Figure 5a and is plotted in Figure 5b as a function of the number of charges exiting the ion trap. Note that the pulsed ion current transmission decreased as the total number of ions transmitted through the collisional quadrupole increased. This trend is indicative of increased radial expansion of the ion packet due to the increased space charge effects and the associated ion losses on the conductance limit orifices and in the elements of the electrostatic Einzel lens. In comparison, total ion transmission efficiency of the continuous beam from the ion funnel to the charge collector was ~35%, which also included ion losses due to the low m/z cut off (<200 m/z) in the collisional quadrupole. Further improvements in the transmission of dense ion packets through the quadrupole interface are feasible through more efficient ion focusing at higher residual gas pressures. However, in proteomic experiments, rigorous control over ion populations accumulated in the ion trap can be accomplished using automated gain control,[33] to be described in a subsequent publication.

The linear dynamic range of the ion trap was studied using reserpine solutions at concentrations ranging from 10 nM to 1 μM. Figure 6 shows the intensity of the monoisotopic peak of reserpine normalized to the number of ion trap releases per 1 s TOF acquisition as a function of accumulation time at different concentrations. As indicated in Figure 6, the ion trap has a linear response at accumulation times ≤20 ms independent of sample concentration. The nonlinearities at longer accumulation time are due to the limitation in ion trap charge capacity and increased transmission losses at higher ion densities.

The improved data quality resulting from the use of the ion trap becomes more evident at low concentrations. Figure 7a shows

(33) Schwartz, J. C.; Zhou, X.-G.; Bier, M. E., Finnigan Corporation. Method and Apparatus of Increasing Dynamic Range and Sensitivity of a Mass Spectrometer. U.S. Patent 5,572,022,November 5, 1996.

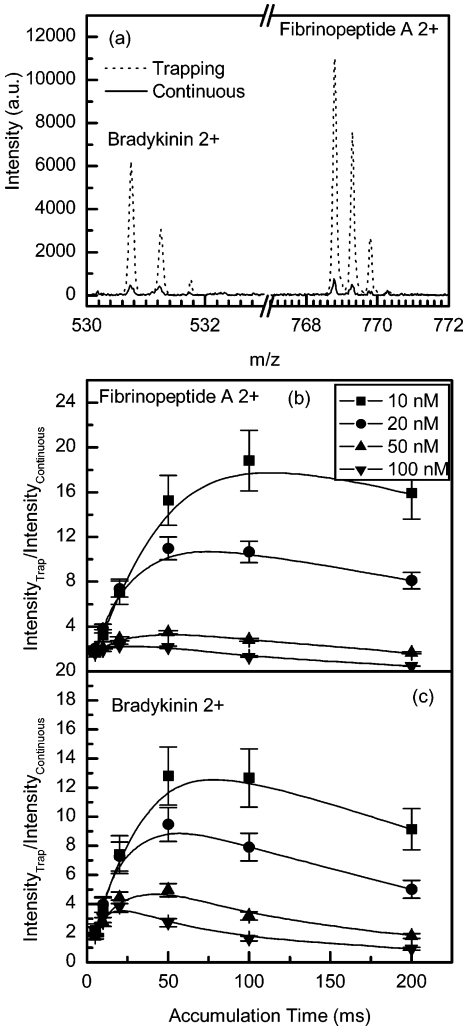

Figure 7. (a) Portions of the mass spectra for ESI of a 10 nM mixture of bradykinin and fibrinopeptide A solution in the continuous and trapping mode (100 ms accumulations, 45 μs extraction time). Lower panels show the ratio of ion signals in the trapping and continuous modes for doubly charged (b) fibrinopeptide A and (c) bradykinin as a function of accumulation time at different concentrations. The mass spectrum acquisition time was 1 s in all cases.

a portion of a mass spectrum for a 10 nM mixture of bradykinin and fibrinopeptide A. For the same TOF acquisition time of 1 s, the intensities of doubly charged bradykinin and fibrinopeptide A ions in the trap mode are more than an order of magnitude higher than those in the continuous (no trapping) mode. In the trapping mode, the mass spectrum corresponds to 20 trap releases per 1s (or a sum of 200 TOF pulses), while in the continuous mode, the mass spectrum is obtained as a sum of 9000 TOF pulses. Figure 7b,c shows the ratios of intensities of doubly charged bradykinin and fibrinopeptide A ions in the trapping and continuous modes as a function of the accumulation time at different analyte concentrations. The trends shown in Figure 7b,c indicate that the intensities of doubly charged bradykinin and fibrinopeptide A exceeded those from the continuous beam by a factor of 13−20-fold at a concentration of 10 nM. When the ion population reaches trap capacity, no further increase in sensitivity is expected in the trapping mode. Furthermore, an increase in accumulation time results in lower duty cycle (and signal) as fewer ion packets are introduced to the TOF MS per unit time, as illustrated in Figure 7b,c at longer accumulation times.

Table 1. Signal-to-Noise Ratio (S/N) and Noise Level for Bradykinin and Fibrinopeptide A

	bradykinin 2+ 530.75 amu		fibrinopeptide A 2+ 768.85 amu	
	S/N	noise[a]	S/N	noise
continuous	15.4	32.1	49.8	14.3
trapping[b]	534.9	11.8	988.8	13.5
ratio	34.6	0.4	19.9	0.9

[a] The noise is in units of mass spectrum intensity (arbitrary units) and is calculated as an average intensity in an m/z segment located 1 Da to the left from the analyte peak. [b] The accumulation time is 100 ms.

Sensitivity improvement in the trapping mode is also related to the more efficient ion desolvation and the resulting reduction of chemical background. The S/N values and noise levels for the data acquired with a 10 nM mixture of bradykinin and fibrinopeptide A are listed in Table 1. Although Figure 7c indicates a ~13-fold signal enhancement for bradykinin in the trapping mode as compared to that obtained in the continuous regime, the actual S/N gain was ~35 due to a 3-fold lower chemical background. The reduction in noise reported in Table 1 is most likely related to the gentle (relatively slow) declustering of solvated ions during their extended accumulation in the trap.[34] A desolvation mechanism in the ion trap is expected to involve water/solvent cluster heating as a result of collisions with neutral gas assisted by the rf field. The rf heating of ions is also promoted by the dc electric field that drives ions to locations with increased effective potential resulting in more efficient activation.

The enhancements in S/N are thus attributed to a combination of an increase in the number of transmitted ions to the TOF detector due to ion accumulation, to more efficient desolvation of the analyte ions, and to removal of chemical background peaks following the desolvation of smaller ions in the ion trap. Since most of the solvent ions are in the low m/z range, a more pronounced background noise reduction is observed in the lower m/z range. We have also evaluated trap performance in the higher m/z range (up to m/z 2000) in experiments with a 1 μM mixture of polyethylene glycol (MW_{aver} 600) and ultramark (MW_{aver} 1600). Polymer solutions were chosen to avoid detection of multiply charged species, typical for ESI of biomolecules. It was found that ion accumulation in the trap resulted in 2- to 3-fold greater signal intensities for higher m/z ultramark ions as compared to those obtained in the continuous mode. The S/N enhancement due to the reduction in the chemical background plays an important role in improving the instrument limit-of-detection (LOD). Figure 8a,b shows portions of the mass spectra obtained for a 0.1 nM solution of neurotensin in both continuous and trapping modes. The solution was infused at a flow rate of 60 nL/min and both mass spectra were acquired over a 3 s period, corresponding to 300 zmol of analyte introduced. The mass spectrum in Figure 8a reveals pronounced chemical background peaks at every m/z, which is common for TOF MS operating in the continuous mode. Figure 8b shows a mass spectrum in which the background noise

(34) Van Berkel, G. J.; Glish, G. L.; McLuckey, S. A. *Anal. Chem.* **1990**, *62*, 1295−1299.

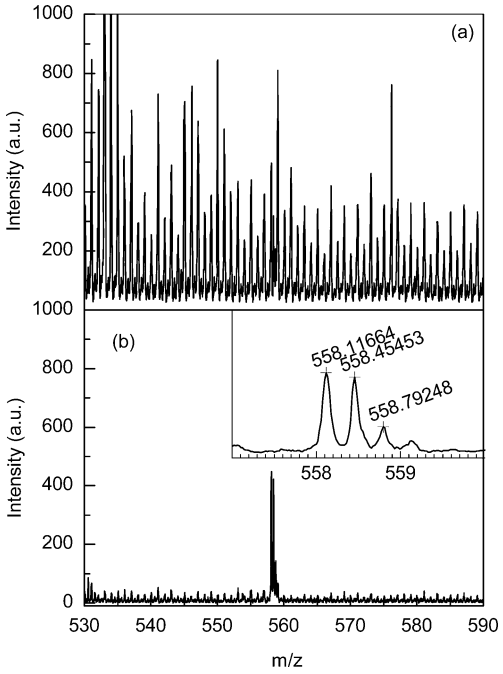

Figure 8. Improvement in the signal-to-noise ratio (S/N) of $[M + H_3]^{3+}$ for ESI of a 0.1 nM of neurotensin solution: (a) continuous regime and (b) trapping mode. Accumulation time = 100 ms, extraction time = 70 μs. In both the continuous and trapping modes, the sample infusion rate was 60 nl/min and TOF acquisition time was 3 s.

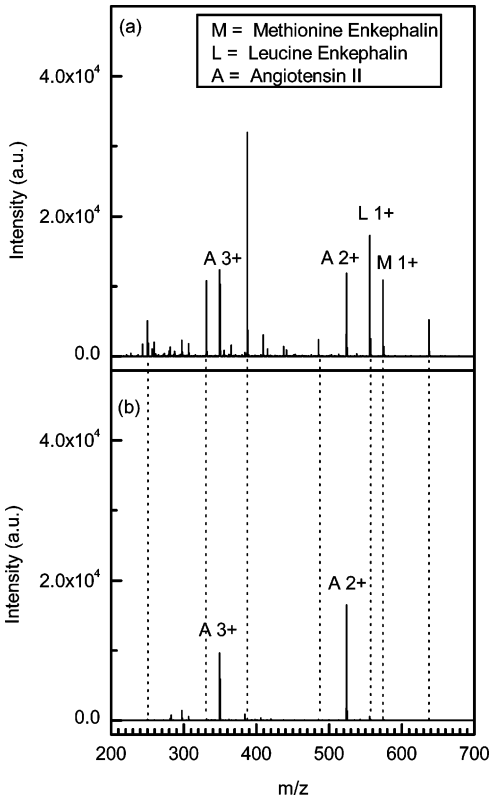

Figure 9. Portions of the mass spectra from ESI of a 28 ng/mL solution of peptides (methionine enkephalin, leucine enkephalin, and angiotensin II) at different ejection times. Trapping conditions: (a) accumulation time = 50 ms, ejection time = 100 μs, and trap dc gradient = 4 V/cm; (b) accumulation time = 50 ms, ejection time = 40 μs, and trap dc gradient = 4 V/cm.

is suppressed and the S/N is 37-fold enhanced. Although it is possible to reduce such solvent related chemical background by greater activation (e.g., heating) in the ESI interface, this measure can also lead to dissociation of analyte species and thus decreased sensitivity.

Because of the relatively high pressure (1 Torr) and the applied dc gradient, a trapped ion cloud exhibits mobility separation during ejection from the trap. As a result, multiply charged ions are separated from their singly charged counterparts in the ejection step. Since mobility is directly related to charge state and inversely proportional to the collisional cross section,[35] multiply charged ions tend to exit the ion trap faster as illustrated in Figure 9a,b. The mixture of peptides was ejected from the ion trap using two different gate opening events: 100 μs (Figure 9a) and 40 μs (Figure 9b). Limiting the extraction time to 40 μs led to discrimination against singly charged species because of their longer drift time through the gate. This effect is exemplified with the singly charged peak at m/z 387.2. The intensity of this peak decreased by 2 orders of magnitude when the extraction time was shortened from 100 μs (Figure 9a) to 40 μs (Figure 9b). A similar effect was also observed for other singly charged species shown in Figure 9a,b.

The controlled separation of multiply charged species from singly charged ones by changing the extraction time could be used to improve the S/N in proteomic experiments with multiply charged tryptic peptides. Gating the ion trap for a period of 40 μs not only substantially decreased the noise level and suppressed the singly charged species but also improved the S/N of multiply charged species by more than an order of magnitude. This approach is advantageous over other methods in which 50−85% of multiply charged species can be lost to suppress singly charged species.[30]

CONCLUSIONS

We developed and characterized an ion trap operating at pressures that enable seamless interfacing to atmospheric pressure ionization sources. The trap operating pressure can also be further increased[27] for, e.g., more efficient coupling to mobility separations. For example, in the current arrangement, the ion trap is characterized by an extraction time of 40 μs for multiply charged ions and 100 μs for singly charged species. We found that an increase in pressure slowed the ion cloud release from the ion trap as a result of enhanced viscous effects. To address the increased drag effects, we implemented further modifications in the trap design that resulted in significantly improved IMS-TOF performance (to be reported in the subsequent publication).

In the current study, the performance of TOF MS was examined in both trapping and continuous modes. In the continuous mode, TOF MS provides a high pulsing rate of ~10 kHz, and given sufficient ion current, each successive TOF pulse can deliver ions to the detector. In the trapping mode, only 100−1000 ion packets are delivered to the TOF detector over the same acquisition period. However, packets of ions accumulated in the trap are characterized by higher charge density than those in the continuous mode. Therefore, to more fully realize the advantages

(35) McDaniel, E. W.; Mason, E. A. *The Mobility and Diffusion of Ions in Gases*; John Wiley and Sons: New York, 1973.

of ion accumulation, the TOF acquisition system should provide a linear detection response to multiple ions within a single TOF digitizer bin, which implies benefit from the implementation of a fast multibit ADC-based data acquisition system.

Last, the improved S/N in the trapping mode resulted from a combination of several factors that contributed to an increase in signal intensity and a decrease in the chemical background level. Ion accumulation in the trap appeared to be particularly advantageous at very low analyte concentrations. The ion packets exiting the trap are characterized by higher ion densities and, therefore, result in higher S/N values. In addition, the ion trap facilitates more efficient desolvation of ions resulting in substantial reduction in background noise and further S/N improvement.

ACKNOWLEDGMENT

Portions of this research were supported by the U.S. Department of Energy (DOE) Office of Biological and Environmental Research, the National Institute of Allergy and Infectious Diseases (NIH/DHHS) through interagency agreement Y1-AI-4894-01, and the National Cancer Institute (NCI) through Grant CA126191. Experimental work was performed in the Environmental Molecular Sciences Laboratory, a DOE national scientific user facility at the Pacific Northwest National Laboratory (PNNL) in Richland, Washington. PNNL is operated by Battelle for the DOE under Contract No. DE-AC05-76RLO 1830.

SUPPORTING INFORMATION AVAILABLE

Additional information as noted in text. This material is available free of charge via the Internet at http://pubs.acs.org.

Received for review May 24, 2007. Accepted July 26, 2007.

AC071091M